The Influence of the Molecular Dipole on the Electronic Structure of Isomeric Icosahedral Dicarbadodecaborane and Phosphacarbadodecaborane Molecular Films

Snjezana Balaz,[†,‡] A. N. Caruso,[†] N. P. Platt,[§] D. I. Dimov,[§] N. M. Boag,[†,§] J. I. Brand,[‡] Ya. B. Losovyj,[†,⊥] and P. A. Dowben*[,†]

Department of Physics and Astronomy and the Nebraska Center for Materials and Nanoscience, Behlen Laboratory of Physics, University of Nebraska, P.O. Box 880111, Lincoln, Nebraska 68588-011, College of Engineering and Technology, N245 Walter Scott Engineering Center, 17th & Vine Streets, University of Nebraska-Lincoln, Lincoln, Nebraska 68588-0511, Functional Materials, Institute for Materials Research, Cockcroft Building, University of Salford, Salford M5 4WT, United Kingdom, and Center for Advanced Microstructures and Devices, Louisiana State University, 6980 Jefferson Highway, Baton Rouge, Louisiana 70806

Received: January 16, 2007; In Final Form: February 16, 2007

We compare the molecular films of three different isomers of *closo*-dicarbadodecaborane (orthocarborane (1,2-$C_2B_{10}H_{12}$), metacarborane (1,7-$C_2B_{10}H_{12}$), paracarborane (1,12-$C_2B_{10}H_{12}$)) and two related icosahedral cage molecules, 1-phospha-2-carbadodecaborane (1,2-$PCB_{10}H_{11}$) and 1-phospha-7-carbadodecaborane (1,7-$PCB_{10}H_{11}$) adsorbed on a variety of substrates. While the experimental electronic structure from combined photoemission and inverse photoemission studies of the molecular films are in good agreement with semiempirical calculations for the isolated molecule, there is a shift in the chemical potential for each molecule. The experimental position of the molecular chemical potential implicates an influence of both interface and adsorbate dipole.

1. Introduction

For many large molecular adlayers, including a number of organic and metal−organic species, the energy level alignment (of the adsorbate) is dependent on the interfacial electronic structure and the interfacial dipole layer.[1−8] While generally the substrate work function plays little role in directly determining the energy level placement,[8] charge transfer,[9,10] and adsorbate molecular interactions with the substrate,[8,11] the adsorbate induced work function change can have a sufficiently large influence that can overcome any effect of the substrate work function. To study the influence of the interface dipole layer, one can still try to study adsorbates on a variety of surfaces with different work functions, but the role of the interfacial chemical interactions makes such studies generally ambiguous.[8,11] Moreover, the dipole orientation of the adsorbate, i.e., the molecular orientation of the adsorbate relative to the surface normal, does matter.[12−13] The icosahedral *closo*-carboranes provide an opportunity to explore that influence of the dipole on adsorbate energy level alignment, as this family of molecules are similar in size, chemistry, and electronic structure, but the different carborane and phosphacarborane isomers provide a wide range of molecular dipoles,[14−15] as summarized in Table 1.

The comparison of the theoretical[16−30] and experimental[25−30] electronic structure, as well as the vibrational modes[31−34] for the various isomers of the closo-carboranes has a rich history. For the isolated molecules, the trends expected from theory seem to be born out in experiment with only slight differences observed between the various carboranes, although *closo*-1,12-dicarbadodecaborane (paracarborane) does have a somewhat greater stability and symmetry than the other icosahedral isomers of *closo*-$C_2B_{10}H_{12}$.

TABLE 1: Experimental Dipole Moments of the Carboranes, Compared with the Values Calculated Using MNDO (*), Restricted Hartree−Fock Employing the 6−31g Basis Set (#) and B3LYP Using the 6-311 g(d,p) Basis Set (†).[45]

molecule	experimental dipole moment (Debyes)	calculated dipole moment (Debyes)
orthocarborane (1,2-$C_2B_{10}H_{12}$)	4.53 ± 0.05 (14)	4.30* 4.42#
metacarborane (1,7-$C_2B_{10}H_{12}$)	2.85 ± 0.05 (14)	2.73* 2.79#
paracarborane (1,12-$C_2B_{10}H_{12}$)	0.00 (14)	0*#
orthophosphacarborane (1,2-$PCB_{10}H_{11}$)	3.87 ± 0.06 (15)	3.55†
metaphosphacarborane (1,7-$PCB_{10}H_{11}$)	2.39 ± 0.03 (15)	2.24†

There is a clear need for this comparison to be revisited in light of the recent comparisons of *closo*-1,7-dicarbadodecaborane (metacarborane) molecular films and *closo*-1,2-dicarbadodecaborane molecular films (orthocarborane)[29] as well as the comparison of *closo*-1,2-dicarbadodecaborane molecular films with *closo*-1-phospha-2-carbadodecaborane molecular films.[35] While the molecular films of the different isomers of *closo*-dicarbadodecaborane ($C_2B_{10}H_{12}$) appear to show similar gaps between the highest occupied molecular orbital (HOMO) and lowest unoccupied molecular orbital (LUMO), surprisingly the placement of the chemical potential in *closo*-1,7-dicarbadodecaborane (1,7-$C_2B_{10}H_{12}$, metacarborane) films differs significantly from the placement of the Fermi level in the HOMO−LUMO gap for *closo*-1,2-dicarbadodecaborane films (1,2-$C_2B_{10}H_{12}$ referred to as orthocarborane).[29,36] This difference in the placement of the molecular orbitals and the effective change

* Corresponding author phone: 402-472-9838; fax: 402-472-2879; e-mail: pdowben@unl.edu.
† Behlen Laboratory of Physics, University of Nebraska.
‡ Walter Scott Engineering Center, University of Nebraska.
§ University of Salford.
⊥ Louisiana State University.

10.1021/jp0703760 CCC: $37.00
Published on Web 06/01/2007

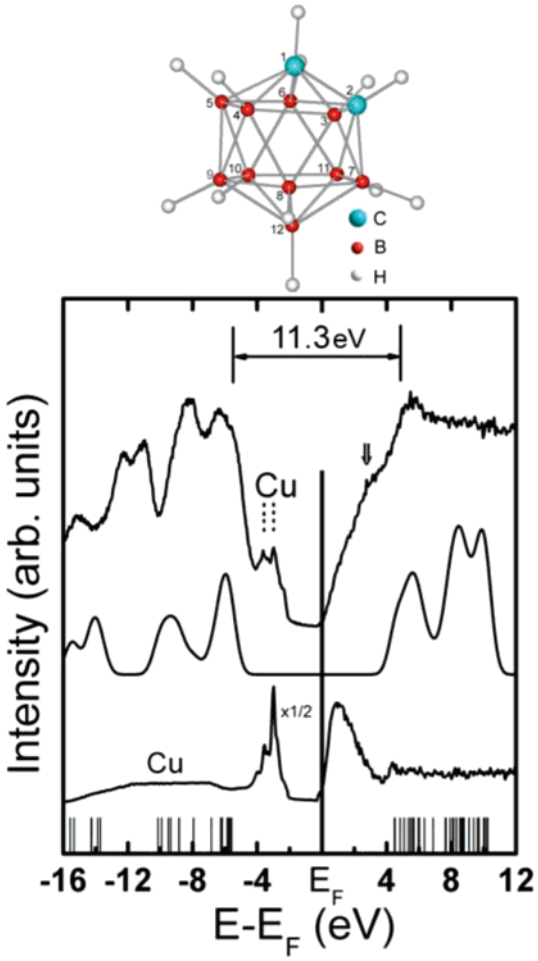

Figure 1. Combined photoemission (PES, left) and inverse photoemission spectroscopy (IPES, *right*) results of *orthocarborane* on copper. Bottom vertical lines represent semiempirical PM3, while the middle line is calculated density of states for each molecule. The bottom experimental spectra correspond to the clean Cu(100) substrate (for reference) while the top spectra are of the adsorbed orthocarborane molecular film. At the top of the spectra there is schematic of the molecule. The photoemission was taken with a photon energy of 30 eV.

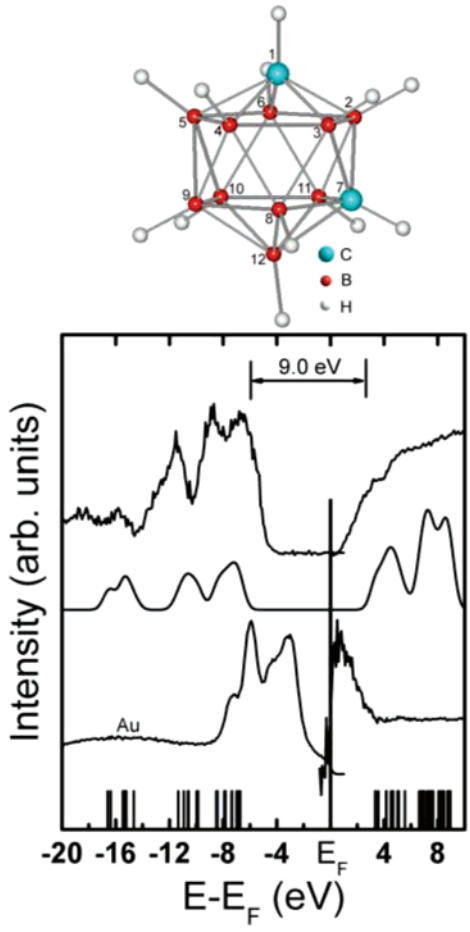

Figure 2. Combined photoemission (PES, left) and inverse photoemission spectroscopy (IPES, right) results of *metacarborane* on gold. Bottom vertical lines represent semiempirical PM3, while the middle line is calculated density of states for each molecule. The bottom experimental spectra correspond to the clean Au substrate (for reference) while the top spectra are of the adsorbed metacarborane molecular film. At the top of the spectra there is schematic of the molecule. The photoemission was taken with a photon energy of 65 eV.

in the placement of the free molecule chemical potential with respect to the substrate Fermi level, E_F, is difficult to understand, as both molecules have identical electron counts and point group symmetry.

By expanding the comparison of the closo carboranes to five closo-carboranes with varying molecular dipoles, we provide compelling evidence that the placement of the adsorbate free molecule chemical potential, relative to the Fermi level of the substrate, is partly correlated with the adsorbate dipole. Molecules used in this comparative study are orthocarborane (*closo*-1,2-dicarbadodecaborane or 1,2-$C_2B_{10}H_{12}$), metacarborane (*closo*-1,7-dicarbadodecaborane or 1,7-$C_2B_{10}H_{12}$), paracarborane (*closo*-1,12-dicarbadodecaborane or 1,12-$C_2B_{10}H_{12}$), orthophosphacarborane (*closo*-1-phospha-2-carbadodecaborane or 1,2-$PCB_{10}H_{11}$), and metaphosphacarborane (*closo*-1-phospha-7-carbadodecaborane or 1,2-$PCB_{10}H_{11}$). These are all icosahedral cage molecules containing ten boron (BH) vertices and either two carbon (CH) vertices or, in case of the phosphacarboranes, one carbon (CH) vertex and one phosphorus (P) vertex (see Figures 1−5).

2. Experimental Section

7-Me_3N-7-$CB_{10}H_{12}$ was prepared from decaborane[37a] and converted first to 1,2-$PCB_{10}H_{11}$ and then to 1,7-$PCB_{10}H_{11}$ by the methodology of Todd and Little.[37b] The sublimed crystalline 1,7-$PCB_{10}H_{11}$ was recrystallized from ethanol and resublimed at 48 °C (0.01 mm Hg) in 45% yield. All the isomers of $C_2B_{10}H_{12}$, i.e., orthocarborane (*closo*-1,2-dicarbadodecaborane or 1,2-$C_2B_{10}H_{12}$), metacarborane (*closo*-1,7-dicarbadodecaborane or 1,7-$C_2B_{10}H_{12}$), paracarborane (*closo*-1,12-dicarbadodecaborane or 1,12-$C_2B_{10}H_{12}$), were purchased from either Katchem or Aldrich and resublimed prior to use, with purity in all cases confirmed by NMR spectroscopy. NMR spectra were obtained on a Bruker AVANCE400 operating at ^{1}H 400.1 MHz, ^{31}P 161.9 MHz, ^{13}C 100.6 MHz, and ^{11}B 128.38 MHz. Proton and carbon spectra were referenced to solvent, boron spectra to an insert of $BF_3{\cdot}Et_2O$ (0.0 ppm) and phosphorus spectra to an insert of $P(OPh)_3$ (126.5 ppm). NMR 1,7-$PCB_{10}H_{11}$ (C_6D_6): ^{11}B 4.6 (B_{12}, J_{BH} = 161 Hz), −1.6 (B5 J_{BH} = 154 Hz), −3.1 (B9/10, J_{BH} = 159 Hz), −7.1 (B4/6 + B8/11, J_{BH} = 163 Hz), −9.9 (B2/3, J_{BH} = 174 Hz, J_{BP} = 38 Hz); ^{31}P{^{1}H} −75.8 ppm; ^{1}H/^{1}H{^{11}B}-32.97 (s, H9/10 + H12), 2.59 (s, H8/11), 2,47 (br d, H5, $^2J_{HP}$ = ∼16 Hz), 2.40 (s, H7), 2.37 (d, H2/3 or H4/6, $^2J_{HP}$ ∼23 Hz), 2.24 (d, H4/6 or H2/3, $^2J_{HP}$ ∼22 Hz); ^{13}C{^{1}H} 65.6. The assignment of the boron and proton resonances was confirmed by ^{11}B{^{1}H}-^{11}B{^{1}H} and ^{1}H{^{11}B}-^{11}B{^{1}H} COSY spectra.

The molecular thin film sample preparation and subsequent spectroscopies were carried out in two ultrahigh vacuum (UHV) chambers with base pressures of 5×10^{-11} Torr. The Fermi

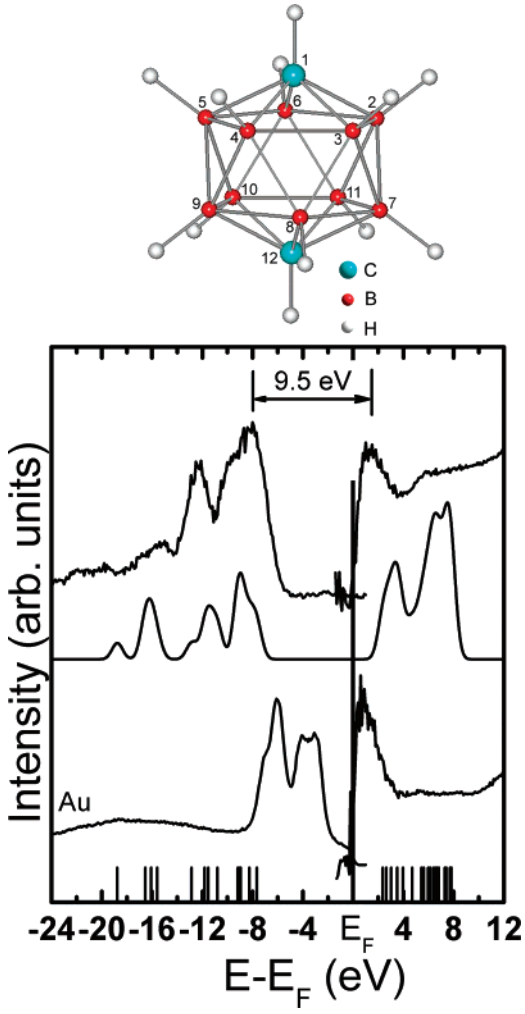

Figure 3. Combined photoemission (PES, left) and inverse photoemission spectroscopy (IPES, right) results of *paracarborane* on gold. Bottom vertical lines represent semiempirical PM3, while the middle line is calculated density of states for each molecule. The bottom experimental spectra correspond to the clean Au substrate (for reference) while the top spectra are of the adsorbed paracarborane molecular film. At the top of the spectra there is schematic of the molecule. The photoemission was taken with a photon energy of 65 eV.

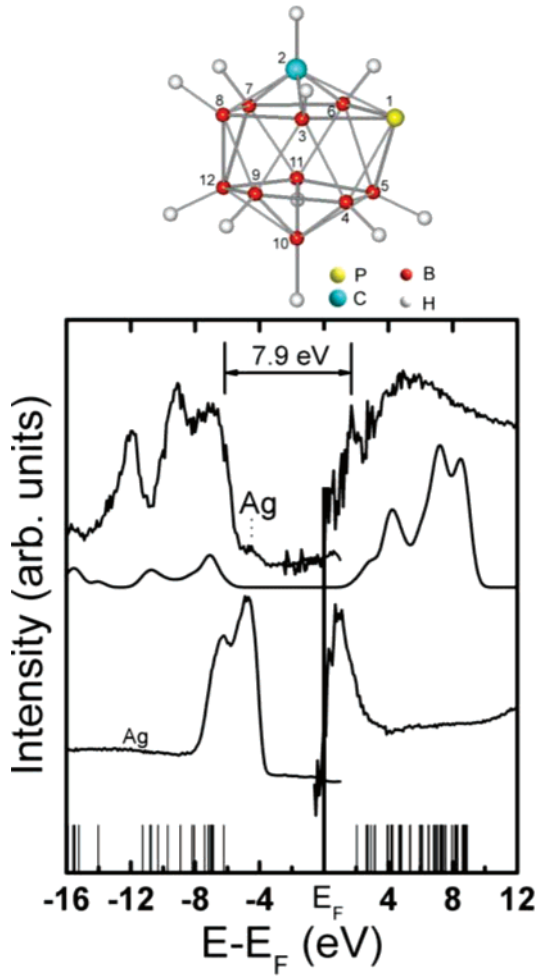

Figure 4. Combined photoemission (PES, left) and inverse photoemission spectroscopy (IPES, right) results of *orthophosphacarborane* on silver. Bottom vertical lines represent semiempirical PM3, while the middle line is calculated density of states for each molecule. The bottom experimental spectra correspond to the clean Ag(100) substrate (for reference) while the top spectra are of the adsorbed orthophosphacarborane molecular film. At the top of the spectra there is schematic of the molecule. The photoemission was taken with a photon energy of 65 eV.

level was established from the clean, well-ordered, substrates as appropriate. The experimental binding energies are referenced to the substrate Fermi level throughout this work. For the inverse photoemission spectroscopy (IPES), a Geiger−Müller detector fitted with a SrF_2 window of 9.5 eV pass energy was used[29,35,36,38,39] together with an Erdman−Zipf electron gun.[40] The overall energy resolution was ~0.40 eV. All IPES spectra were collected with the electron gun at normal incidence, and the detector positioned at 45° off the surface normal. The photoemission spectra were taken with the photoelectrons collected along the surface normal, as has been described elsewhere.[29,35,38,39,42] Photoemission spectroscopy (PES) data were taken using a photon energy of 65 eV, unless otherwise stated, from synchrotron light at the Center for Advance Microstructures and Devices,[42] Baton Rouge, LA, dispersed by a 3 m toroidal grating monochromator at normal incidence.

Prior to growth of the molecular films, the metal substrates (Cu(100), Co(111), Ag(100), or Au(111)) were cleaned using Ar^+ ion bombardment and annealed. The clean surfaces were characterized by photoemission. The substrates were then cooled to 150−200 K, and the molecular films grown through exposure to the molecular carborane vapor, sublimed from the solid powder and admitted to the vacuum chambers through a standard leak valve, at 2×10^{-6} Torr, as described previously.[29,35,36,38,39,42] Because sticking coefficients vary from one carborane to the next,[29,35] a range of molecular film coverages was studied for each molecule, with the nominal film thickness ranging from 4 to 12 molecular layers, as judged by the attenuation of the substrate photoemission signal. The exception is the metaphosphacarborane, which exhibited Stranski−Krastanov growth of the molecular film, and thus shows strong substrate contributions in photoemission even for very thick molecular films (as discussed below). The actual coverage dependence of some of carboranes has been discussed elsewhere (orthocarborane,[29,38,39] metacarborane,[29] orthophosphacarborane,[35] and metaphosphacarborane[43]). The electronic structure of molecular paracarborane did not show any significant coverage dependence for coverages up to 20 molecular monolayers. In all cases, film thickness dependence studies were undertaken to make sure that this was not the origin of the differences in electronic structure noted below.

3. Theory

The ground state molecular orbital energies were calculated using a PM3 model calculation with the HyperChem package

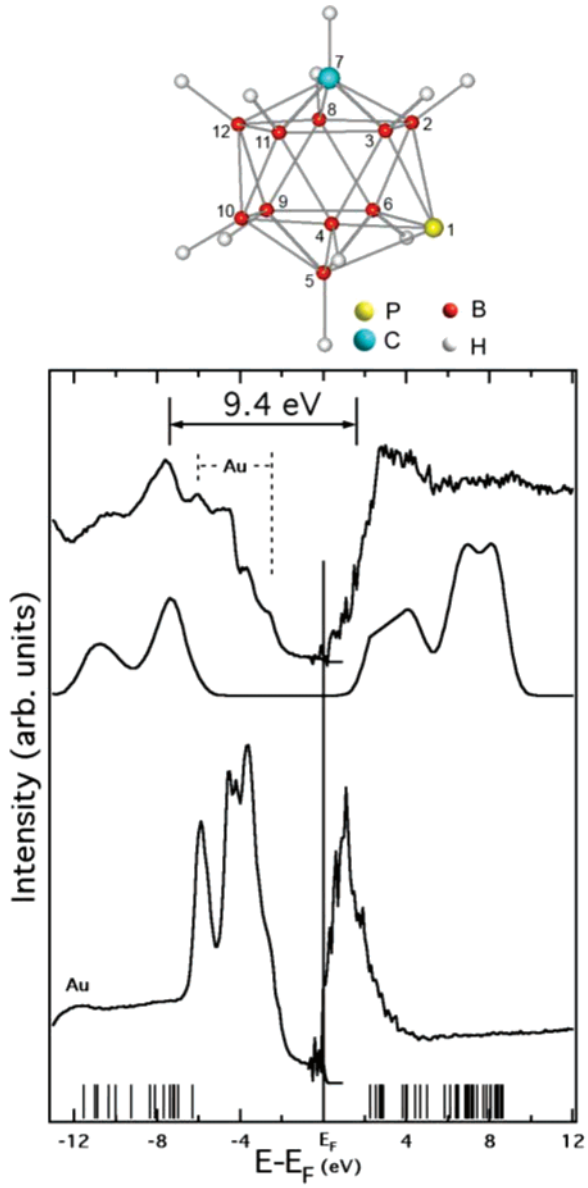

Figure 5. Combined photoemission (PES, left) and inverse photoemission spectroscopy (IPES, right) results of *metaphosphacarborane* on gold. Bottom vertical lines represent semiempirical PM3, while the middle line is calculated density of states for each molecule. The bottom experimental spectra corresponds to the clean gold substrate (for reference) while the top spectra are of the adsorbed orthocarborane molecular film. At the top of the spectra there is schematic of the molecule. The photoemission was taken with a photon energy of 21.5 eV.

and compared to prior MNDO calculations of our own and others,[16,17,25,29,36,40] as summarized in the Supporting Information tables. These semiempirical calculations of occupied and unoccupied molecular orbitals were undertaken following geometry optimization and the calculation of the lowest restricted Hartree−Fock (RHF) energy states. The results of both semiempirical calculations are similar and have been found to provide good agreement with photoemission and inverse photoemission experiments, with regard to ascertaining the HOMO−LUMO gap. The calculated HOMO−LUMO gap of 10.97 eV (MNDO) to 10.1 eV (PM3) is within 3−12% of the experimental gap of 11.3 ± 0.3 eV for orthocarborane on copper. The estimated HOMO−LUMO gap of 10.87 eV (MNDO) to 10.0 eV (PM3) is within 11−21% of the experimental gap of 9.0 ± 0.3 eV for metacarborane on gold. The calculated HOMO−LUMO gap of 10.0 eV (PM3) is close to the experimental gap of 9.5 ± 0.3 eV for paracarborane on gold. The calculated HOMO−LUMO gap of 8.3 eV (PM3) is also close to the experiment value of 8.0 ± 0.3 eV for orthophosphacarborane on gold and 7.9 ± 0.3 eV for orthophosphacarborane on silver. The calculated HOMO−LUMO gap of 8.5 eV (PM3) is close to the observed experimental gap of 9.4 ± 0.3 eV for metaphosphacarborane on gold. This is summarized in Figures 1−5 and in the Supporting Information data. For adsorption on cobalt, the observed HOMO−LUMO gap is 33 ± 1 % (MNDO) to 22 ± 1% smaller than expected for both metacarborane and orthocarborane adsorption, and this has been attributed to the stronger interaction with cobalt substrates.[29] Density functional theory tends to predict a HOMO−LUMO gap far smaller than observed in the combined photoemission and inverse photoemission experiments.

The calculated densities of states were obtained by applying equal Gaussian envelopes of 1 eV width to each molecular orbital binding energy (to account for the solid-state broadening in photoemission) and then summing. In addition, a rigid energy shift was applied to the calculated electronic structure, as noted below. There are no corrections for finite temperature, solid-state effects, matrix element effects (symmetry and selection rules), final state photoemission effects, or multi-configurational final state effects in the theory, so the theory must be taken only as a guide. As a result, peak intensities differ from experiment, particularly for inverse photoemission, and the binding energies in photoemission generally deviate from the ground state orbital energy calculations more significantly for states farther from chemical potential (see the Supporting Information tables for more extensive detail). These semiempirical ground state calculations for the free molecule provide a qualitative guide to interpreting the photoemission and inverse photoemission features, as indicated in the Supporting Information data, in spite of severe limitations and the simplistic methodology.[16,17,25,29,35,36,39]

We find good agreement between MNDO[44] as well as between PM3[35] and experimental bond lengths. In addition, several schemes in Gaussian 03 were used to calculated the dipole moments,[45] as summarized in Table 1.

4. Comparison of the Adsorbed Molecular Film with Theory

Each closo-carborane was adsorbed on several different substrates. Orthocarborane was molecularly adsorbed on Cu(100), Ag(100), and Co(111); metacarborane on Ag(100), Au(111), and Co(111); paracarborane on Ag(100) and Au(111), and both phosphacarboranes on Ag(100) and Au(111). For each closo-carborane, the appropriate substrate photoemission and inverse photoemission features were suppressed, after exposure, because of the limited mean free path of the photoelectron. This is illustrated in Figure 1 (orthocarborane), Figure 2 (metacarborane), Figure 3 (paracarborane), Figure 4 (orthophosphacarborane) and Figure 5 (metaphosphacarborane).

The two 1,2-disubstituted molecules differ from the other closo-carboranes in that at the onset of multilayer growth, under some circumstances, a weak state appears within the HOMO−LUMO gap at approximately 0.7 eV above the Fermi level for orthophosphacarborane[35] and at approximately 3 eV above the Fermi level in orthocarborane molecular films.[29,36,38,39] Since there is no counterpart to this state in the molecular orbitals of orthophosphacarborane (1,2-$PCB_{10}H_{11}$) or orthocarborane (1,2-$C_2B_{10}H_{12}$), and because with rapid multilayer adsorption this state is not observed, we have concluded that it is an exopoly-

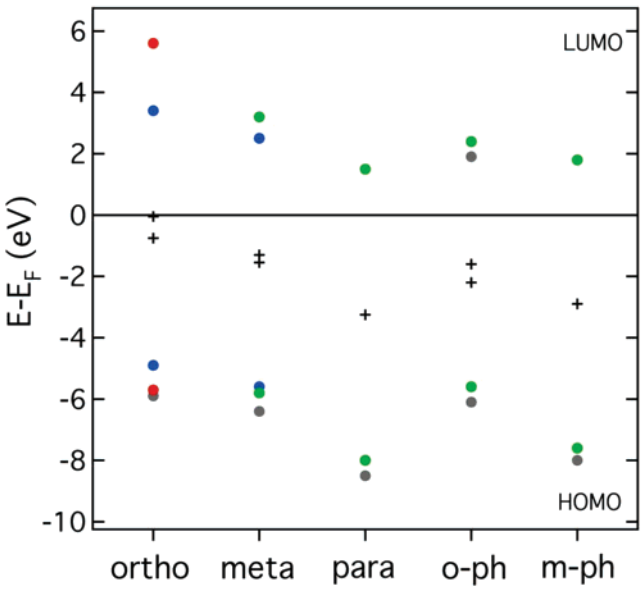

Figure 6. A comparison of the placement of highest occupied molecular orbitals (HOMO), and lowest unoccupied molecular orbitals (LUMO) for the carboranes determined in this work. The filled circles represent the experimental values from photoemission and inverse photoemission: green on Au, dark gray on Ag, blue on Co, red on Cu, and plus (+) is the placement of the experimental HOMO−LUMO midgap points.

hedral state and possibly extra molecular.[29,35,36,38,39] This state could arise from defects, molecular misorientation, or from the loss of exopolyhedral hydrogen. An alternative possibility is an extrinsic state arising from cluster−cluster hybridization.

A fairly rigid shift of the orbital energies is required to match the experimental points. This corresponds to an energy shift of roughly 5.5 eV for adsorbed orthocarborane, roughly 4.6 eV for adsorbed metacarborane, roughly 2.4 eV for adsorbed paracarborane, roughly 3.8 eV for adsorbed orthophosphacarborane, and roughly 3.6 eV for adsorbed metaphosphacarborane. These shifts cannot be ascribed to the substrate work function, and therefore, they must be largely related to the adsorbate and the adsorbate interactions with the substrate. Since the different closo-carboranes should be (and are indeed) chemically and electronically similar, the adsorbate dipole moment is implicated.

5. The Adsorbate Dipole Moment

The differences in the electronic structure of adsorbed orthocarborane, metacarborane, paracarborane, orthophosphacarborane, and metaphosphacarborane, as noted above, can be also seen in the placement of the molecular chemical potential (i.e., the HOMO−LUMO gap center) with respect to the Fermi level of the substrate. We have plotted the experimental energies of the highest occupied molecular orbital (HOMO), the lowest molecular orbital (LUMO), and the center of the HOMO−LUMO gap for each adsorbate substrate combination studied thus far, referenced to the substrate Fermi level, in Figure 6.

While, as noted above, the HOMO−LUMO gaps generally agree with theory (excluding the studies on cobalt surfaces), the placement of the molecular chemical potential is closest to the substrate Fermi level for orthocarborane (regardless of substrate) and farthest for paracarborane (Figure 6). The carbene bond, and the possibility of multiple bond character between the two carbon atoms, invoked earlier to explain this result,[29] has been excluded by the phosphacarborane results,[35] as well as the results for paracarborane. This experimental shift in the adsorbate molecular orbitals with respect to the substrate

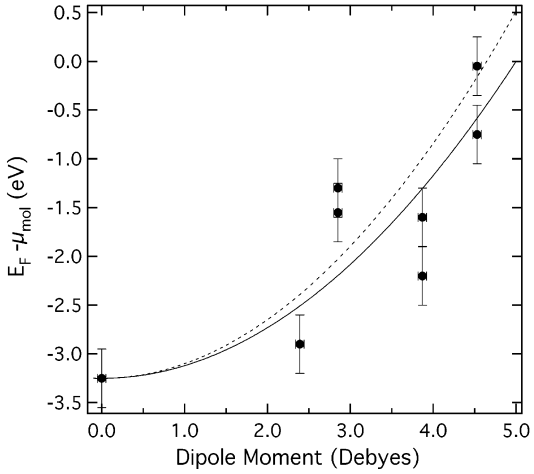

Figure 7. Chemical potential shift (experimental HOMO−LUMO midgap points) of each carborane with respect to the Fermi level of the substrate as a function of the experimental molecular dipole moment (Table 1). The fits indicate fits of eq 1 to all the data (solid line) and the fit to the *closo*-$C_2B_{10}H_{12}$ carboranes alone (dashed line); in both cases the fitting has been done with the assumption that the data for paracarborane is a stable point (i.e., given much greater weight in the fit) as this value should not be influenced by any possible dipole canting. From the design of our experiments, we treat k and R^3 (of eq 1) as constants.

Fermi level seems to better follow the trend of the adsorbate permanent electric dipole moment (Table 1). This is illustrated in Figure 7.

By plotting the center of the experimental adsorbate HOMO−LUMO gap with respect to the substrate Fermi level, we see that this energy shift generally follows the permanent dipole moment of the adsorbate. In other words, the molecular chemical potential is altered by different interactions upon adsorption, and this interaction leads to differences in the energy level alignment with respect to the Fermi energy of the substrate (Figure 7). This has been predicted in other molecular adsorbates[7,8,46−48] and should follow the potential shift due to dipolar interactions,[49−50] i.e.,

$$E_{\mathrm{int}}^{\mathrm{dip}}(R) = k\frac{\mu^2}{R^3} \qquad (1)$$

where μ is the dipole moment, R is the distance from the substrate surface, and k is a constant. For films of similar thickness, as is the case here, deviations from this μ^2 relationship can occur because of a dipole cant away from the surface normal, which can be taken into account through the following relationship:[2]

$$E_{\mathrm{int}}^{\mathrm{dip}}(R) = k\frac{\mu^2}{R^3}(1 + \cos^2\theta) \qquad (2)$$

but only if the favored "tilt" angle θ, the dipole orientation with respect to the surface normal, is known. Further complications in the form of a tilt angle between adsorbate dipoles would further alter eq 2.

It should be noted that this treatment ignores differences in intermolecular interactions, strong substrate interactions (chemisorption) and the interface dipole caused by the different substrates that will give rise to deviations from a μ^2 relationship. Significantly, the variation in chemical potential of the phosphacarboranes may also be understood in terms of this dipole interaction model, although the chemical potential shifts ex-

hibited are consistently lower than predicted. The size of the phosphorus in the carborane cage is known to cause distortion of the cage and this may well result in some internal adjacent icosahedral ordering within the film that is not observed in the carboranes in which the constituent vertex atoms are similarly sized. Such ordering could well give rise to differing preferred dipole orientations with respect to the surface as well as subtle bonding effects within the films themselves which is manifested in the position of the chemical potential.

In spite of these deficiencies, the simple model of dipole interaction (eq 1) works surprisingly well: the smaller the adsorbate dipole of each closo-carborane, the closer the placement of the substrate Fermi level to the lowest unoccupied adsorbate molecular orbital. This change in the placement of the molecular orbital levels relative to the substrate Fermi level seems to generally vary as the adsorbate dipole squared. Thus there appears to be a chemical interaction mediated by the interaction of the adsorbate dipole with the image dipole within the conducting substrate. We think it is unlikely that the simple model of dipole interaction will be applicable to both conducting and nonconducting substrates, as the conductivity of the substrate does have some influence on dipole alignment.[51]

Another explanation for the data would be to argue that the work function change, induced by the adsorbate, is the principle cause of the shift in the molecular energy levels. This is an interfacial dipole argument,[52,53] and in this case, the work function change $\Delta\phi$, varies linearly with the interface dipole μ along the surface normal as follows:

$$\Delta\phi = \frac{-\mu\sigma}{\epsilon_0} \tag{3}$$

where σ is the dipole density per unit area and ϵ_0 is the permittivity of free space. While we cannot conclusively distinguish between the two models (eqs 1 and 3) on the basis of our data alone, as the carboranes likely lead to a small work function increase and the molecular adsorption must then be very weak, this latter explanation seems less plausible.

The dipole interaction models above appear generally applicable to the carboranes, but require that the carboranes are weakly bound molecular adsorbates. It should be recognized that these are relative weakly bound adsorbates with negligible sticking coefficients for adsorption above 220 K and tendencies to undergo facile desorption at room temperature under ultrahigh vacuum conditions.[29,35,38,39,43]

6. Crystallographic Data and Structure of 1,7-$PCB_{10}H_{11}$

While possible deviations from the expected μ^2 relationship in eq 1, as seen in Figure 7, do require detailed knowledge of the favored dipole orientation, it is clear that molecular crystals of the phosphacarboranes are not composed of randomly oriented molecular icosahedra. The larger phosphorus atom in the phosphacarboranes results in a greater distortion from a regular icosahedron than caused by a carbon atom in the carborane cage. Thus, it is conceivable that the orientation of the PCB_{10} icosahedra are not completely random and this may well affect dipole orientation within the molecular film. Indeed, deviations of the dipole orientation, with respect to the surface normal, almost certainly occur with the phospacarborane molecular films. Such a postulate is supported by the observation that while most of the closo-carboranes are grown roughly layer by layer, the phosphacarboranes, in particular the metaphosphacarborane (1,7-$PCB_{10}H_{11}$), grow via a Stranski−Krastanov growth mode.[43] This does implicate an intermolecular interaction that can overcome the substrate interaction with increasing film thickness.

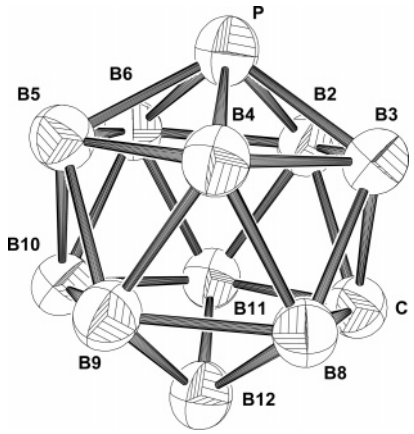

Figure 8. The structure of *closo*-1-phospha-7-carbadodecaborane (1,7-$PCB_{10}H_{11}$) with the ellipsoids set at the 50% probability level and hydrogen atoms omitted for clarity. The unique positions are *arbitrarily* labeled as P and C and the remaining atoms as B using the conventional numbering scheme.

To further explore this issue, we have carefully studied the structure of molecular 1,7-$PCB_{10}H_{11}$.[54] Data were collected using a Siemens *P*4 diffractometer at −50 °C on a colorless triangular prism ($0.5 \times 0.5 \times 0.25$ mm^3) mounted on a glass pin. After data collection, the structure was solved by Direct Methods in the cubic space group Pa-3 and found to be isomorphous to 1,2-$PCB_{10}H_{11}$ with only two independent atom positions.[35] The structure was, therefore, refined analogously using P, C, and B atoms in the appropriate occupancy ratio (1:1:10) constrained to identical positional and thermal parameters. Hydrogen atoms were identified and their positional parameter refined using an 11/12 occupancy with the thermal parameter tied to the appropriate heavy atom. The derived molecular structure is shown in Figure 8 with the two unique positions arbitrarily assigned as P and C; the remaining atoms being labeled as B in the appropriate numbering scheme.

Within the 1,7-$PCB_{10}H_{11}$ icosahedral structure, there are 30 interatomic bonds; 5 P−B bonds, 5 C−B bonds, and 20 B−B bonds. The high symmetry of the disordered structure results in only five (erroneously described as three in ref 35) unique bonding distances, 1.8603(19), 1.8605(19), 1.8607(19), 1.8353(16), and 1.877(2) Å. Averaging over all 30 bonds gives a value of 1.859 Å, essentially identical to the value found for 1,2-$PCB_{10}H_{11}$.[35] The weighted averages of the icosahedral cage bond lengths calculated here (1.84 Å) and by using ab initio theory (1.85 Å) are in good agreement with the experimental values of 1.83−1.88 Å.

In further refining the experimental data, we see that in the packing of the molecular icosahedra into the molecular cubic lattice, the positions generated by the two unique atom positions show an interesting ordering. We have colored the atoms in Figure 9 to show which of the two unique positions occur within the icosahedra, and how they are oriented within the crystal. One position generates a pair of parallel triangular faces (orange) and the other a central belt (gray). The "orange" to "orange" atom distance (1.877(2) Å) is significantly longer than the "gray" to "gray" atom distance (1.8353(16) Å). The three intermediate distances (1.8603(19), 1.8605(19), 1.8607(19) Å) arise from orange to gray bonds. It is, therefore, likely that there is a small but significant preference for the P to sit in an orange position rather than in a gray position. Additionally, the orange atom

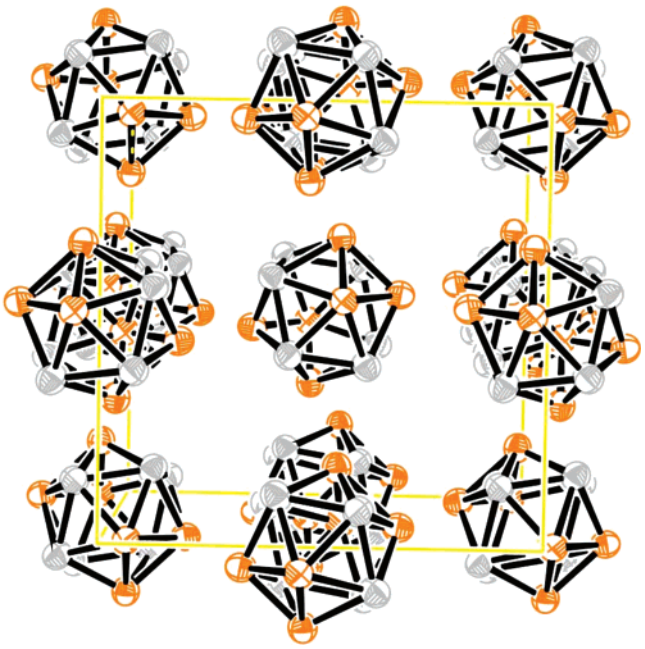

Figure 9. The unit cell structure of *closo*-1-phospha-7-carbadodecaborane (1,7-$PCB_{10}H_{11}$) with the ellipsoids set at the 50% probability level and hydrogen atoms omitted for clarity. The atoms are colored to show which of the two unique positions generate the various positions within the icosahedra (see text). One position generates a pair of parallel triangular faces (orange) and the other a central belt (gray). On the basis of the interatomic distances, there appears to be a small but significant preference for the P to sit in the orange atom positions that point along the axes in the unit cell.

positions sit along the axes in the unit cell (see Figure 9). Given the tendency for the phosphorus to occupy the orange atom positions, it is probable that the phosphorus substituent does result in some ordering of the icosahedra in the solid state and that this ordering will not always favor a dipole orientation along the surface normal. Exactly the same situation is found for 1,2-$PCB_{10}H_{11}$.[35] Given the closer distances of C−C, B−B, and B−C bonds, identifying unique positions for carbon from the crystallographic data of orthocarborane (1,2-$C_2B_{10}H_{12}$), metacarborane (1,7-$C_2B_{10}H_{12}$), or paracarborane (1,12-$C_2B_{10}H_{12}$) would present an even greater challenge. Although the bulk crystal structure may differ from that found in thin films of 1,7-$PCB_{10}H_{11}$, we do have evidence of preferential orientation from light polarization dependent photoemission and strong evidence of band structure from angle-resolved photon energy dependent photoemission, with critical points that appear to be in agreement with Figure 9.

7. Substrate Dependence

While we find that the permanent adsorbate dipole moment will alter the placement of the molecular orbitals with respect to the substrate, there are also the expected affects of substrate induced interface dipoles.[1] Other groups[1−8] have varied different built-in interface potentials at the surface by changing the substrate and thus changing the work function of the substrate.

We have not studied each and every one of the five closo-carboranes on all four substrates, but in general, we find that the molecular chemical potential is closer to the substrate Fermi level for adsorbates on Au(111) compared to Ag(100) and Co-(111), and Cu(100) compared to Ag(100), as seen from Figure 6. Since the work function of Au(111) (5.3 eV[55]) > Co(111) (5.0 eV[56]) > Ag(100) (4.64 eV[57]) > Cu(100) (4.59 eV[58]), this imperfectly suggests that the greater the work function (and the greater the interface dipole), the farther the molecular adsorbate chemical potential from the substrate Fermi level. This mirrors our more compelling evidence that the greater the adsorbate dipole, the farther the molecular adsorbate chemical potential from the substrate Fermi level. We note that the work function does not always influence the molecular orbital alignment with respect to the substrate Fermi level in a well-defined fashion. Kera et al.[6] did not see the shifts in the molecular orbital energy alignment (relative to the substrate Fermi level) with molecules without the permanent dipole moment, and adsorbate interactions can overcome the influence of the interface dipole.[11] In any case, the interface dipole resulting from the substrate work function does not dominate the influence of the adsorbate permanent dipole on the alignment of the molecular orbitals with respect to the substrate Fermi level.

8. Summary

The smaller the adsorbate dipole of each closo-carborane, generally the closer the placement of the substrate Fermi level to the lowest unoccupied adsorbate molecular orbital. The data suggest that not only does the interface dipole, as has been discussed for large molecular adsorbates,[6−8] but also the adsorbate dipole influences the placement of molecular levels. The role of the adsorbate dipole is in general agreement with expectations based on dipole interactions for adsorbates on conducting substrates. The agreement with the model dipoles interacting with a conducting substrate may be imperfect because of dipole misorientation with respect to the surface normal (for which we have some additional indications) that will result in deviations from the models of dipole interactions with a conducting substrate. The results here are complementary to the increased recognition of the role of dipole screening on the dielectric relaxation in solids[59] and molecular thin films.

This work can be expanded to include the study of many more closo-carboranes and a wider variety of substrates. Possibilities include isomers of $AsCB_{10}H_{11}$ and $SbCB_{10}H_{11}$ as well as a variety of other main group substituted closo-carboranes.

Acknowledgment. This work was supported by the National Science Foundation through grant CHE-0415421, the Office of Naval Research (grant N00014-06-1-0616), the Defense Advanced Projects Agency, and through the Chief Technical Officer, Intelligence Technology Innovation Center of the United States Intelligence Community, the EPSRC (NPP) and the ORS (DID). The Center for Advanced Microstructures and Devices is supported by the Louisiana Board of Regents. This material is based upon work funded in part by the U.S. government and any opinions, findings, conclusions, or recommendations expressed in this paper, are those of the authors and do not necessarily reflect the views of the U.S. government.

Supporting Information Available: Additional details may be found in 5 tables. Crystallographic information is also available. This material is available free of charge via the Internet at http://pubs.acs.org.

References and Notes

(1) Ishii, H.; Sugiyama, K.; Ito, E.; Seki, K. *Adv. Mater.* **1999**, *11*, 605−625.
(2) Zhu, X. Y. *Surf. Sci. Rep.* **2004**, *56*, 1−83.
(3) Fukagawa, H.; Yamane, H.; Kera, S.; Okudaira, K. K.; Ueno, N. *Phys. Rev. B* **2006**, *73*, 041302(R).
(4) Munakata, T.; Sugiyama, T.; Masuda, T.; Aida, M.; Ueno, N. *Appl. Phys. Lett.* **2004**, *85*, 3584−3586.
(5) Fukagawa, H.; Yamane, H.; Kera, S.; Okudaira, K. K.; Ueno, N. *J. Electron Spectrosc. Relat. Phenom.* **2005**, *144−147*, 475−477.

(6) Kera, S.; Yabuuchi, Y.; Yamane, H.; Setoyama, H.; Okudaira, K. K.; Kahn, A.; Ueno, N. *Phys. Rev. B* **2004**, *70*, 085304.
(7) Yamane, H.; Honda, H.; Fukagawa, H.; Ohyama, M.; Hinuma, Y.; Kera, S.; Okudaira, K. K.; Ueno, N. *J. Electron Spectrosc. Relat. Phenom.* **2004**, *137*−*140*, 223−227.
(8) Knupfer, M.; Paasch, G. *J. Vac. Sci. Technol., A* **2005**, *23*, 1072−1077.
(9) Gorgoi, M.; Zahn, D. R. T. *Appl. Surf. Sci.* **2006**, *252*, 5453−5456.
(10) Schwieger, T.; Peisert, H.; Knupfer, M. *Chem. Phys. Lett.* **2004**, *384*, 197−202.
(11) Caruso, A. N.; Schulz, D. L.; Dowben, P. A. *Chem. Phys. Lett.* **2005**, *413*, 321−325.
(12) Kera, S.; Yamane, H.; Honda, H.; Fukagawa, H.; Okudaira, K. K.; Ueno, N. *Surf. Sci.* **2004**, *566*, 571−578.
(13) Yamane, H.; Yabuuchi, Y.; Fukagawa, H.; Kera, S.; Okudaira, K. K.; Ueno, N. *J. Appl. Phys.* **2006**, *99*, 093705.
(14) Laubengayer, A. W.; Rysz, W. R. *Inorg. Chem.* **1965**, *4*, 1513−1514.
(15) Echeistova, A. I.; Syrkin, Ya, K.; Zakharkin, L. I. *Zh. Strukt. Khim.* **1970**, *11*, 552−552; *J. Struct. Chem.***1970**, *11*, 509−510; Echeistova, A. I.; Syrkin, Ya. K.; Kyskin, V. I.; Zakharkin, L. I.; *Zh. Strukt. Khim*. **1971**, *12*, 728−729; *J. Struct. Chem.* **1971**, *12*, 663−664; Todd, L. J.; Burke, A. R.; Graber, A. R.; Silverstein, H. T.; Storhoff, B. N. *Inorg. Chem.* **1970**, *9*, 2175−2179.
(16) Cheung, C.-C. S.; Beaudet, R. A.; Segal, G. A. *J. Am. Chem. Soc.* **1970**, *92*, 4158−4164.
(17) Dewar, M. J. S.; McKee, M. L. *Inorg. Chem.* **1980**, *19*, 2662−2672.
(18) Lipscomb, W. N.; Koetzle, T. F. *Inorg. Chem.* **1970**, *9*, 2743−2748.
(19) Hoffman, R.; Lipscomb, W. N. *J. Chem. Phys.* **1962**, *36*, 3489−3493.
(20) Guest, M. F.; Hillier, I. H. *Mol. Phys.* **1973**, *26*, 435−452.
(21) Dewar, M. J. S.; McKee, M. L. *Inorg. Chem.* **1978**, *17*, 1569−1581.
(22) Green, T. A.; Switendick, A. C.; Emin D. *J. Chem. Phys.* **1988**, *89*, 6815−6822.
(23) Stone, A. J.; Alderton, M. J. *Inorg. Chem.* **1982**, *21*, 2297−2302.
(24) Brint, P.; Cronin, J. P.; Seward, E.; Whelan, T. *J. Chem. Soc., Dalton Trans.* **1983**, 975−980.
(25) Brint, P.; Sangchakr, B.; McGrath, M.; Spalding, T. R.; Suffolk, R. J. *Inorg. Chem.* **1990**, *29*, 47−52.
(26) Aflatooni, K.; Gallup, G. A.; Burrow, P. D. *J. Phys. Chem. A* **2002**, *106*, 4703−4708.
(27) Hitchcock, A. P.; Wen, A. T.; Lee, S.; Glass, J. A.; Spencer, J. T.; Dowben, P. A. *J. Phys. Chem.* **1993**, *97*, 8171−8181.
(28) Hitchcock, A. P.; Urquhart, S. G.; Wen, A. T.; Kilcoyne, A. L. D.; Tyliszczak, T.; Rühl, E.; Kosugi, N.; Bozek, J. D.; Spencer, J. T.; McIlroy, D. N.; Dowben, P. A. *J. Phys. Chem. B* **1997**, *101*, 3483−3493.
(29) Caruso, A. N.; Bernard, L.; Xu, B.; Dowben, P. A. *J. Phys. Chem. B* **2003**, *107*, 9620−9623.
(30) Vondrák, T. *Polyhedron*, **1987**, *6*, 1559−1562.
(31) Zhang, M.; Zhao, Y. *J. Mol. Struct.* **2001**, *545*, 105−110.
(32) Leites, L. A. *Chem. Rev.* **1992**, *92*, 279−323.
(33) Vinogradova, L. E.; Kyskin, V. I.; Leites, L. A.; Zakharkin, L. I. *Izv. Akad. Nauk SSSR, Ser. Khim.* **1972**, 2436−2440, *Russ. Chem. Bull.* **1972**, *21*, 2372−2375; Leites, L. A.; Vinogradova, L. E.; Kalinin, V. N.; Zakharkin, L. I. *Izv. Akad. Nauk SSSR, Ser. Khim.* **1968**, 1016−1014, *Russ. Chem. Bull.* **1968**, *17*, 970−977; Bukalov, S. S.; Leites, L. A.; Aleksanyan, V. T. *Izv. Akad. Nauk SSSR, Ser. Khim.* **1968**, 929−930, *Russ. Chem. Bull.* **1968**, *17*, 896−896; Salam, A.; Deleuze, M. S.; Francois, J.- P. *Chem.l Phys.* **2003**, *286*, 45−61.
(34) Schroeder, H.; Heying, T. L.; Reiner, J. R. *Inorg. Chem.* **1963**, *2*, 1092−1096; Alexander, R. P.; Schroeder, H. *Inorg. Chem.* **1963**, *2*, 1107−1110; Grafstein, D.; Dvorak, J. *Inorg. Chem.* **1963**, *2*, 1128−1133; Zakharkin, L. I.; Stanko, V. I.; Brattsev, V. A.; Chapovskii, Yu. A. *Dokl. Akad. Nauk SSSR* **1964**, *157*, 1149−1154; Papetti, S.; Heying, T. L. *J. Am. Chem. Soc.* **1964**, *86*, 2295−2295.
(35) Balaz, S.; Dimov, D. I.; Boag, N. M.; Nelson, K.; Montag, B.; Brand, J. I.; Dowben, P. A. *Appl. Phys. A: Mater. Sci. Process.* **2006**, *84*, 149−159.
(36) Caruso, A. N.; Billa, R. B.; Balaz, S.; Brand, J. I.; Dowben, P. A. *J. Phys.: Condens. Matter*. **2004**, *16*, L139−L146.
(37) (a) Plešek, J.; Jelínek, T.; Drdáková, E.; Hemánek, S.; Štíbr, B. *Collect. Czech. Chem. Commun*., **1984**, *49*, 1559−1562. (b) Little, J. L.; Moran, J. T.; Todd, L. J. *J. Am. Chem. Soc*. **1967**, *89*, 5495−5496; Knoth, W. H.; Little, J. L.; Lawrence, J. R.; Scholer, F. D.; Todd, L. J. *Inorg. Synth*. **1968**, *11*, 33−41.
(38) Zeng, H.; Byun, D.; Zhang, J.; Vidali, G.; Onellion, M.; Dowben, P. A. *Surf. Sci.* **1994**, *313*, 239−250.
(39) McIlroy, D. N.; Zhang, J.; Dowben. P. A.; Heskett, D.; *Mater. Sci. Eng., A* **1996** *217/218*, 64−68; McIlroy, D. N.; Waldfried, C.; McAvoy, T.; Choi, J.; Dowben, P. A.; Heskett, D. *Chem. Phys. Lett.* **1997**, *264*, 168−173.
(40) Zhang, J.; McIlroy, D. N.; Dowben, P. A.; Zeng, H.; Vidali, G.; Heskett, D.; Onellion, M. *J. Phys.: Condens. Matter* **1995**, *7*, 7185−7194.
(41) Erdman, P. W.; Zipf, E. C. *Rev. Sci. Instum.* **1982**, *53*, 225−227.
(42) Hormes, J.; Scott, J. D.; Suller, V. P. *Synchrotron Radiat. News* **2006**, *19*, 27−30.
(43) Balaz, S.; Boag, N. M.; Platt, N. P.; Dimov, D. I.; Brand, J. I.; Dowben, P. A. *Mater. Res. Soc. Symp. Proc.* **2007**, in press.
(44) Lee, S.; Dowben, P. A.; Wen, A. T.; Hitchcock, A. P.; Glass, J. A., Jr.; Spencer, J. T. *J. Vac. Sci. Technol., A* **1992**, *10*, 881−885.
(45) Frisch, M. J.; Trucks, G. W.; Schlegel, H. B.; Scuseria, G. E.; Robb, M. A.; Cheeseman, J. R.; Montgomery, J. A., Jr.; Vreven, T.; Kudin, K. N.; Burant, J. C.; Millam, J. M.; Iyengar, S. S.; Tomasi, J.; Barone, V.; Mennucci, B.; Cossi, M.; Scalmani, G.; Rega, N.; Petersson, G. A.; Nakatsuji, H.; Hada, M.; Ehara, M.; Toyota, K.; Fukuda, R.; Hasegawa, J.; Ishida, M.; Nakajima, T.; Honda, Y.; Kitao, O.; Nakai, H.; Klene, M.; Li, X.; Knox, J. E.; Hratchian, H. P.; Cross, J. B.; Bakken, V.; Adamo, C.; Jaramillo, J.; Gomperts, R.; Stratmann, R. E.; Yazyev, O.; Austin, A. J.; Cammi, R.; Pomelli, C.; Ochterski, J. W.; Ayala, P. Y.; Morokuma, K.; Voth, G. A.; Salvador, P.; Dannenberg, J. J.; Zakrzewski, V. G.; Dapprich, S.; Daniels, A. D.; Strain, M. C.; Farkas, O.; Malick, D. K.; Rabuck, A. D.; Raghavachari, K.; Foresman, J. B.; Ortiz, J. V.; Cui, Q.; Baboul, A. G.; Clifford, S.; Cioslowski, J.; Stefanov, B. B.; Liu, G.; Liashenko, A.; Piskorz, P.; Komaromi, I.; Martin, R. L.; Fox, D. J.; Keith, T.; Al-Laham, M. A.; Peng, C. Y.; Nanayakkara, A.; Challacombe, M.; Gill, P. M. W.; Johnson, B.; Chen, W.; Wong, M. W.; Gonzalez, C.; Pople, J. A. *Gaussian 03*, revision C.02; Gaussian, Inc.: Wallingford, CT, 2004.
(46) Schwieger, T.; Peisert, H.; Knupfer, M.; *Chem. Phys. Lett.* **2004**, *384*, 197−202.
(47) Yamane, H.; Fukagawa, H.; Kera, S.; Okudaira, K. K.; Ueno, N. *Synth. Met.* **2005**, *152*, 297−300.
(48) Campbell, I. H.; Kress, J. D.; Martin, R. L.; Smith, D. L.; Barashkov, N. N.; Ferraris, J. P. *Appl. Phys. Lett.* **1997**, *71*, 3528−3530.
(49) Desjonquères, M.−C.; Spanjaard, D. *Concepts in Surface Physics*; 2nd ed.; Springer−Verlag: New York, 1998; pp 515−525.
(50) Topping, J. *Proc. R. Soc. London, Ser. A* **1927**, *114*, 67−72.
(51) Duan, C.-G.; Mei, W. N.; Yin, W.-G.; Liu, J.; Hardy, J. R.; Ducharme, S.; Dowben, P. A. *Phys. Rev.* B **2004**, *69*, 235106.
(52) Langmuir, I. *J. Am. Chem. Soc.* **1932**, *54*, 2798−2832.
(53) Taylor, J. B.; Langmuir, I. *Phys. Rev.* **1933**, *44*, 423−458.
(54) SHELX97 Programs for Crystal Structure Analysis (Release, 97−2). Sheldrick, G. M. Institüt für Anorganische Chemie der Universität, Tammanstrasse 4, D-3400 Göttingen, Germany, 1998; WINGX. L.J. Farrugia, L.J. *J. Appl. Crystallogr*. **1999**, *32*, 837−838; ORTEP3 for Windows. Farrugia, L.J. *J. Appl. Crystallogr*. **1997**, *30*, 565.
(55) Potter, H. C.; Blakely, J. M. *J. Vac. Sci. Technol.* **1975**, *12*, 635−642.
(56) Eastman, D. E. *Phys. Rev. B* **1970**, *2*, 1−2.
(57) Dweydari, A. W.; Mee, C. H. B. *Phys. Status. Solidi A* **1975**, *27*, 223−230.
(58) Gartland, P. O.; Berge, S.; Slagsvold, B. J. *Physica Norvegica* **1973**, *7*, 39−49.
(59) Jonscher, A. K. *J. Mater. Sci.* **1997**, *32*, 6409−6414.